QUARTERLY JOURNAL OF THE ROYAL METEOROLOGICAL SOCIETY
Q. J. R. Meteorol. Soc. **135**: 1697–1714 (2009)
Published online 9 October 2009 in Wiley InterScience
(www.interscience.wiley.com) DOI: 10.1002/qj.459

Do tropical cyclones intensify by WISHE?

Michael T. Montgomery[a,b,*], Nguyen Van Sang[c], Roger K. Smith[c] and John Persing[d]

[a] *Dept. of Meteorology, Naval Postgraduate School, Monterey, CA, USA*
[b] *NOAA's Hurricane Research Division, Miami, FL, USA* [†]
[c] *Meteorological Institute, University of Munich, Munich, Germany*
[d] *Department of Mathematics, Colorado State University, Fort Collins, CO, USA*

ABSTRACT: In this paper we seek and obtain a basic understanding of tropical cyclone intensification in three dimensions when precipitation and evaporative-cooling (warm rain) processes are included. Intensification with warm rain physics included is found to be dominated by highly localized deep convective structures possessing strong cyclonic vorticity in their cores – dubbed 'Vortical Hot Towers' (VHTs). Unlike previous studies, the findings herein suggest an intensification pathway that is distinct from the 'evaporation–wind' feedback mechanism known as wind-induced surface heat exchange (WISHE), which requires a positive feedback between the azimuthal-mean boundary-layer equivalent potential temperature and the azimuthal-mean surface wind speed underneath the eyewall of the storm. Intensification from a finite-amplitude initial vortex is shown to not require this evaporation–wind feedback process. Indeed, when the surface wind speed in the sea-to-air vapour fluxes is capped at a nominal (trade-wind) value, the vortex still intensifies by the same pathway identified in the main experiments via the generation of locally buoyant VHTs and the near-surface convergence that the VHTs induce within the boundary layer.

The present findings and interpretations challenge the prevailing view that tropical cyclones are premier examples of vortical systems arising from WISHE. Given the potential significance on our understanding of the dynamics of hurricanes, and given the limitations of the present modelling framework, further tests of these predictions are advocated.

KEY WORDS hurricane; typhoon; local buoyancy; vorticity; vortical hot tower

Received 20 November 2008; Revised 7 May 2009; Accepted 11 May 2009

1. Introduction

This is one of a series of papers examining idealized experiments of tropical cyclone intensification in three dimensions using a cloud-representing model. The aim of this paper is to obtain a more complete understanding of the thermodynamic processes that support the intensification of the vortex.

A prototype problem for tropical cyclone intensification considers the evolution of a prescribed, initially cloud-free, axisymmetric, baroclinic vortex over a warm ocean on an f-plane. It is presumed that the initial vortex has become established and has maximum swirling winds near the ocean surface as a result of some genesis process. One paradigm for the intensification process invokes a positive feedback between the wind speed near the surface and the evaporation of water from the underlying ocean, *which depends on the wind speed* (Emanuel *et al*., 1994, section 5a). This paradigm is based on axisymmetric reasoning and is supported by axisymmetric models (Ooyama, 1969; Rotunno and Emanuel, 1987; Craig and Gray, 1996; Gray and Craig, 1998). Moreover, it has achieved widespread acceptance in tropical weather briefings, dynamic meteorology textbooks (e.g. Holton, 2004; Asnani, 2005), and current literature (Lighthill, 1998; Smith, 2003; Molinari *et al.*, 2004; Montgomery *et al.*, 2006).

Except near the centre, the near-surface wind speed in a tropical cyclone increases with decreasing radius. This increase is typically accompanied by an increase in near-surface specific humidity, which leads to a negative radial gradient of equivalent potential temperature, θ_e, near the surface and hence throughout the boundary layer by vertical mixing processes. On account of frictional convergence, air parcels in the inner core rise upwards and outwards from the boundary layer and as they do so they conserve their θ_e, carrying with them an imprint of the near-surface radial gradient of θ_e into the interior of the vortex. Since the rising air rapidly saturates, this radial gradient of θ_e implies a negative radial gradient of virtual temperature. Thus, in the cloudy region at least, the vortex is warm cored. The air rising out of the boundary layer conserves its absolute angular momentum also. Consequently, as it moves outwards it spins more slowly, which broadly accounts for the observed decrease of the tangential wind speed with height. Scaling arguments show that, where the radial flow component is small compared with

*Correspondence to: Michael T. Montgomery, Dept. of Meteorology, Naval Postgraduate School, Monterey, CA, USA. E-mail: mtmontgo@nps.edu
[†]The contribution of M. T. Montgomery was prepared as part of his official duties as a United States Federal Government employee.

the tangential component, the tangential wind field is in thermal wind balance with the virtual temperature field. The model vortex as described so far may not be steady: for one thing the surface is a sink of absolute angular momentum and a stationary flow would require a source that is equal and opposite; for another thing, the vortex may be dynamically (i.e. symmetrically) unstable.

Suppose now that for some reason the negative radial gradient of specific humidity increases in the boundary layer. This would increase the negative radial gradient of θ_e, both in the boundary layer and in the cloudy region of the vortex aloft, and thereby warm the vortex core in this region. Assuming that the vortex remains in thermal wind balance during this process, the negative vertical shear of the tangential wind will increase. Emanuel (1986) presents arguments to show that this increase leads to an increase in the maximum tangential wind speed *at the top of the boundary layer* (e.g. Montgomery *et al*., 2006, Equation A1). Assuming that this increase translates to an increase in the surface wind speed, the *surface* moisture flux will increase, thereby increasing further the specific humidity. This increase, however, tends to reduce the thermodynamic disequilibrium in specific humidity between the near-surface air and the ocean surface, unless the saturation specific humidity at the sea surface temperature were to increase approximately in step. The increase in wind speed could help maintain this disequilibrium if there is an associated reduction in surface pressure. (Recall that the saturation specific humidity at the sea surface temperature is approximately inversely proportional to the air pressure.) If the specific humidity (and θ_e) in the boundary layer increases further, it will lead to a further increase in tangential wind speed, and so on.

This positive feedback between the near-surface θ_e and the near-surface wind is our interpretation of the wind-induced surface heat exchange (WISHE) mechanism applied to tropical cyclone amplification (cf. Emanuel *et al*., 1994; Craig and Gray, 1996; Holton, 2004). A schematic of the WISHE mechanism as outlined is presented in Figure 1.[†]

As pointed out by Emanuel *et al*. (1994), this is not a runaway process for the present climate and would cease if the boundary layer were to saturate. Moreover, the import of low-entropy air into the boundary layer, for example by shallow convection, precipitation-induced downdraughts from deep convection, or vortex-scale subsidence, can significantly offset the moistening of the boundary layer by surface fluxes (e.g. Ooyama, 1997; Smith, 2003; Smith and Vogl, 2008). Indeed Emanuel *et al*. (1994) argue that tropical cyclone amplification requires the middle troposphere to become nearly saturated on the mesoscale so that the downdraughts are weak enough not to negate this feedback process.

Perhaps surprisingly, the above arguments are silent about the role of the secondary circulation in the vortex-scale amplification process and because the arguments assume thermal wind balance, the buoyancy, or more precisely the system buoyancy, of the warm core cannot be invoked to 'drive' the secondary circulation. In particular, cloud updraughts have no explicit local buoyancy. (The concepts of *system buoyancy* and *local buoyancy* are discussed by Smith *et al*., 2005.) The role of the mean secondary circulation is addressed in a companion paper by Smith *et al.* (2009; hereafter M3). A related property of the WISHE model is that any latent instability beyond that needed to overcome internal dissipation within cumulus clouds is believed unnecessary and thus irrelevant to the essential dynamics of hurricanes (Rotunno and Emanuel, 1987).

The above interpretation and discussion of the WISHE mechanism are largely consistent with the view in a recent study by Molinari *et al.* (2004):

The wind-induced surface heat exchange (WISHE) theory of Emanuel (1986) and Rotunno and Emanuel (1987) has continued to be refined (e.g. Emanuel, 1989, 1997). The essence of the theory has remained the same, however: the prehurricane vortex must be of finite amplitude to develop, axisymmetry and slantwise neutrality are assumed, and development occurs basically as a feedback between surface wind speed and speed-dependent surface moist entropy flux. The WISHE-based developing hurricane contains no cold downdrafts nor strongly buoyant updrafts, and no asymmetric convection.

Observations show that tropical cyclones are highly asymmetric during their intensification phase. Only the most intense storms exhibit a strong degree of axial symmetry and even then, only in their inner core region. Observations show also that rapidly developing storms are accompanied by 'bursts' of intense convection, which one may surmise possess significant local buoyancy. From this perspective, then, the WISHE theory appears incomplete and the question arises, what are its limitations? In an effort to address this question, Nguyen *et al.* (2008, hereafter M1) carried out a series of high-resolution numerical experiments using a three-dimensional non-hydrostatic mesoscale model to examine the effect of convective structures in the intensification process. The model has a bulk-aerodynamic representation of the air–sea interaction process and, for most of the experiments, employed a simple explicit representation of moist processes that mimics pseudo-adiabatic moist thermodynamics. It was shown that the emergent flow becomes highly asymmetric and dominated by deep convective vortex structures possessing intense cyclonic

[†]More recent work has proposed an alternative version of the WISHE intensification mechanism that tacitly assumes gradient wind balance in the boundary layer (Emanuel, 1997; Gray and Craig, 1998; Frisius, 2006). An expression for the time rate of change of tangential wind at the radius of maximum tangential wind derived by Emanuel (1997, Equation (20)) equates the tangential wind tendency to the sum of three terms, two of which are negative definite. The third term is positive if the radial gradient of an *ad hoc* parameter is negative. This *ad hoc* parameter is introduced to 'crudely represent the effects of convective and large-scale downdraughts, which import low θ_e air into the subcloud layer'. In this version of the WISHE mechanism, intensification requires the radial gradient of this *ad hoc* parameter to be sufficiently negative to offset the other two terms. One weakness of this theory is the lack of a clear physical basis for the *ad hoc* parameter. A second weakness is the assumption of gradient wind balance in the boundary layer (Smith and Montgomery, 2008).

DOI: 10.1002/qj

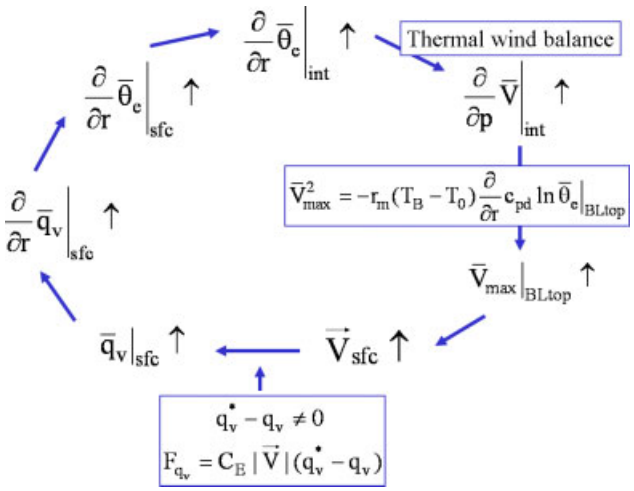

Figure 1. Schematic of the evaporation-wind intensification mechanism known as WISHE as articulated in the Introduction. The pertinent variables are defined in the text and are otherwise standard. Thermal wind balance refers to the axisymmetric thermal wind equation in pressure coordinates that relates the radial gradient of azimuthal-mean θ_e to the vertical shear of the mean tangential velocity. The discussion assumes that for some reason the near-surface azimuthal mean mixing ratio is increased in the core region. This increase leads to an increase in the corresponding mean radial gradient and also an increase in the mean radial gradient of θ_e through the boundary layer. The secondary circulation is imagined to loft this increase in θ_e into the vortex interior thereby warming the core region of the vortex. By the thermal wind relation and its corollary (obtained upon applying a Maxwell thermodynamic relation and then integrating this equation along a surface of constant absolute angular momentum), this increased warmth is invoked to imply an increase in the mean tangential wind at the top of the vortex boundary layer. It is understood here that θ_e values at the boundary-layer top correspond to saturated values (Emanuel, 1986). Turbulent mixing processes in the boundary layer are assumed to communicate this wind speed increase to the surface, and thereby increase the potential for increasing the sea-to-air water vapour flux F_{q_v}. The saturation mixing ratio must increase approximately in step with the putative increase in near-surface q_v so as to maintain a thermodynamic disequilibrium. If this occurs then the surface mixing ratio will increase, thereby leading to a further increase in the mean tangential wind, and so on. This figure is available in colour online at www.interscience.wiley.com/journal/qj

vorticity in their cores, even though the problem as posed is essentially axisymmetric. These vortical hot-plume structures are what have been referred to as vortical hot towers (Hendricks *et al*., 2004; Montgomery *et al*., 2006). The asymmetries in the vortex core are highly sensitive in detail to the boundary-layer moisture distribution and have significant amplitude. When a small random moisture perturbation is added in the boundary layer at the initial time, the pattern of evolution of the flow asymmetries is dramatically changed and a non-negligible spread in the local and azimuthally averaged intensity results. We found, *inter alia*, that the flow on the convective scales exhibits a degree of randomness and only those asymmetric features that survive in an ensemble average of many realizations can be regarded as robust. Similar findings were reported by Shin and Smith (2008) in the context of a minimal hurricane model.

A significant finding of the calculations in M1 is that intensification proceeds with little attenuation even when the wind-speed dependence of the latent and sensible heat fluxes is capped at a value comparable to combined surface fluxes in the undisturbed Trades (on the order of $150\,\mathrm{W\,m^{-2}}$). However, when the moisture flux is suppressed altogether, there is no amplification of the system-scale winds and the initial conditional available potential energy (CAPE) is rapidly consumed. These findings affirm the essential role of sea-to-air fluxes of water vapour in the intensification process. However, they question the necessity of the WISHE mechanism (increasing sea-to-air moisture flux with wind surface speed) as articulated above.

Of course, with the simple pseudo-adiabatic representation of deep convection, precipitation-induced downdraughts are excluded. For this reason, M1 examined briefly the effects of warm rain, in which downdraughts are operative also. With the inclusion of downdraughts the intensification process is still dominated by VHTs. Furthermore, the rate of intensification as well as the final intensity of the vortex is reduced compared to the pseudo-adiabatic calculations. Notably, when the wind-speed dependence of the surface fluxes is capped again to approximately undisturbed trade-wind values, the vortex still intensifies, but at a reduced rate. The current study is motivated by our desire to further understand these and related warm-rain (no-ice) calculations and their implications.

In the companion paper (M3) two of our three-dimensional experiments are examined further to revisit the axisymmetric aspects of the dynamics of the spin up process. In M3, two mechanisms for spinning up the swirling winds of the tropical cyclone are identified: the first involves convergence of absolute angular momentum within the frictional boundary layer where this quantity is not materially conserved, while the second involves its convergence above the boundary layer where it is conserved. Since VHTs have been suggested to play an important role in both mechanisms (Montgomery *et al.*, 2006), our purpose here is to obtain a more complete understanding of the local and system-scale thermodynamics that support the VHTs and their contribution to the spin-up of the tropical cyclone wind field.

DOI: 10.1002/qj

2. The model configuration

The experiments described below are carried out using a modified version of the Pennsylvania State University–National Center for Atmospheric Research fifth-generation Mesoscale Model (MM5; version 3.6) (Dudhia, 1993; Grell *et al.*, 1995), which is suitable for the study of idealized problems. The model is configured with three domains: a coarse mesh of 45 km grid spacing and two 2-way nested domains of 15 and 5 km grid spacing, respectively. The domains are square and are 5400 km, 1800 km, and 600 km on each side. There are 24 σ-levels in the vertical, seven of which are below 850 hPa. Two experiments employing a fourth domain (300×300 km) have been conducted also to permit increased spatial accuracy down to 1.67 km horizontal grid spacing on the innermost domain. The outer lateral boundary of the largest domain is rigid with zero normal flow through it.

To keep the experiments as simple as possible, we choose the principal physics options to be the same as in M1, namely, a bulk-aerodynamic boundary-layer scheme and either the simplest explicit (pseudo-adiabatic) moisture scheme or the 'warm rain' scheme. In the latter scheme the effects of ice microphysical processes are ignored. These schemes are applied in all domains. For simplicity, no radiative cooling and convective parametrization are employed (except in Experiments 12 and 13, see Table II). The sea surface temperature is set to a constant 27 °C. The initial vortex is axisymmetric with a maximum tangential wind speed of 15 m s^{-1} at the surface at a radius of 135 km. The strength of the initial tangential wind decreases sinusoidally with height, vanishing at the top model level (50 hPa) (Figure 2). In three experiments, the initial maximum tangential wind speed is reduced to 7.5 m s^{-1} in order to test the sensitivity of reducing the initial amplitude on the ensuing vortex evolution when the wind-speed dependence of the surface heat fluxes are capped at a nominal trade-wind value (see below for further details). The temperature field is initialized to be in gradient wind balance with the wind field using the method described by Smith (2006). The far-field temperature and specific humidity are based on an approximation of Jordan's Caribbean sounding during summertime conditions (Figure 1 of M1). All fields are kept fixed at the lateral boundary of the coarsest domain for the time of the simulation (except in Experiments 12 and 13, see Table II).

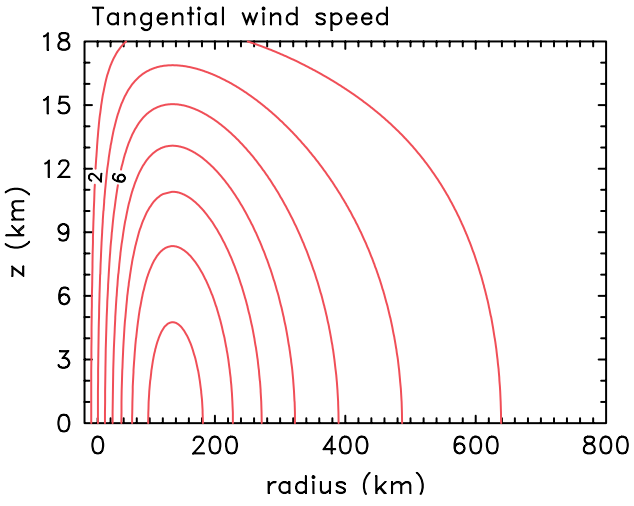

Figure 2. Radius–height contour plot of initial tangential velocity in the main experiments presented. The contour interval is 2 m s^{-1}. This figure is available in colour online at www.interscience.wiley.com/journal/qj

The main experiments here are the warm-rain and pseudo-adiabatic experiments described in M1 (Table I herein). In addition, we have executed a suite of additional experiments (Table II) to investigate the dependence of vortex behaviour on the latent and sensible heat fluxes at the lowest model level. The effects of warm rain are investigated with a capped near-surface relative humidity in the far environment of the vortex as a crude parametrization of shallow convective processes that the current model configuration of MM5 does not represent. In addition, we investigate experiments with a weaker initial vortex, a higher horizontal resolution, and with both of these factors combined. Several physical effects and different model configurations such as radiative cooling, doubly periodic boundary conditions and an initial 'neutral sounding' for the far-field environment have been investigated also. Further, to assess briefly the dependence of our results on the underlying three-dimensionality of the flow, we present two experiments (Experiments 7 and 14) using the axisymmetric Rotunno and Emanuel (1987) model (Table II and Appendix give details).

It proves useful at this juncture to recall that the heat and momentum exchange coefficients (C_k and C_d, respectively) do exhibit some variation for the bulk-aerodynamic boundary-layer scheme in MM5 (e.g. Braun and Tao, 2000, their Table II). The dependence of C_k and C_d on the wind speed, V, at the lowest σ-level enters through the formula of the Richardson number (Ri_{B}) as coded in MM5

$$Ri_{\mathrm{B}} = \frac{g z_{\mathrm{a}}}{\theta_{\mathrm{a}}} \frac{(\theta_{\mathrm{va}} - \theta_{\mathrm{vg}})}{V^2}, \qquad (1)$$

where g denotes gravitational acceleration, z height, θ the potential temperature, and θ_{v} the virtual potential temperature; the subscript a denotes the value at the lowest model level, subscript g at surface. The values of C_k and C_d depend on whether the flow characterized by Ri_{B} is stable ($0 \leq Ri_{\mathrm{B}} \leq 2.75$) or unstable ($Ri_{\mathrm{B}} < 0$) (Grell *et al.*, 1995, provides more details). For the capped experiments the explicit dependence of C_k on wind speed is suppressed by setting $V^2 =$ constant in Ri_{B}. However, this does not render C_k constant because there is still an indirect dependence via the bulk stability, which varies spatially within the vortex. In order to eliminate all variation of C_k, one sensitivity experiment has been conducted wherein C_k is set to a constant of 1.3×10^{-3} for every domain.‡ It is shown in section 5

‡Some support for this experiment that holds C_k constant while allowing C_d to vary is provided in the recent observations of Black *et al.* (2007, their Figures 5 and 6) showing that the drag

DOI: 10.1002/qj

Table I. Warm-rain and pseudo-adiabatic experiments.

No.	Name	Description
1	Warm rain.	Warm rain (control) experiment on an f-plane.
2	Pseudo-adiabatic.	Explicit latent heat release with no water loading or evaporative cooling processes.

Table II. The suite of additional experiments. The initial far-field environment is based on an approximation of Jordan's Caribbean sounding during summertime conditions for Experiments 1–11 and an approximately 'neutral sounding' for Experiments 12–14. Experiments 8–14 are discussed in the Appendix.

No.	Name	Description
3	Capped warm rain.	Surface wind speed is capped at $10\,\mathrm{m\,s^{-1}}$ in formulae for latent and sensible heat fluxes.
4	Capped pseudo-adiabatic.	As Experiment 3, but using pseudo-adiabatic option.
5	Capped RH in outer region and capped warm rain.	As Experiment 3, but the lowest-model-level RH on the outer two domains is capped at 80%.
6	Weak initial vortex, capped warm rain and capped RH in outer region.	As Experiment 5, but the initial $VT_{\max}$ is set to $7.5\,\mathrm{m\,s^{-1}}$ instead of $15\,\mathrm{m\,s^{-1}}$ and the near-surface wind-speed cap is set to $7.5\,\mathrm{m\,s^{-1}}$ for latent and sensible heat fluxes.
7	Rotunno and Emanuel (1987) model with capped fluxes.	As Experiment 3, but the axisymmetric Rotunno and Emanuel (1987) cloud model is used. The surface wind-speed cap is set to $10\,\mathrm{m\,s^{-1}}$ for latent and sensible heat fluxes. See section 5 for details.
8	Weak initial vortex and capped warm rain.	As Experiment 3, but the initial $VT_{\max}$ is set to $7.5\,\mathrm{m\,s^{-1}}$ instead of 15 m s^{-1} and the near-surface wind-speed cap is set to $7.5\,\mathrm{m\,s^{-1}}$ for latent and sensible heat fluxes.
9	Capped warm rain and high resolution.	As Experiment 3, but a fourth domain (300 km square) is added with a horizontal grid spacing of 1.67 km.
10	Weak initial vortex, capped warm rain and high resolution.	As Experiment 8, but a fourth domain (300 km square) is added with a horizontal grid spacing of 1.67 km.
11	Capped RH in outer region, capped warm rain, and constant heat-transfer coefficient.	As Experiment 5, but the heat-transfer coefficient, C_k, is set to 1.3×10^{-3} for all three domains.
12	Warm rain and 'neutral' sounding.	As Experiment 1, but the initial sounding for the far-field environment is obtained from the Rotunno and Emanuel (1987) model 'neutral' state. A Newtonian radiational cooling scheme is employed as in Rotunno and Emanuel (1987) with a cooling time-scale of one day. A doubly periodic boundary condition in x and y is used for the coarsest domain also.
13	Warm rain, 'neutral' initial sounding, capped wind in inner region and no heat fluxes in outer region.	As Experiment 12, but the surface wind speed is capped at $10\,\mathrm{m\,s^{-1}}$ in formulae for latent and sensible heat fluxes within the inner circular region of 300 km radius on fine grid (5 km mesh), and surface heat fluxes are set to zero exterior to 300 km radius from the domain centre and two outer domains.
14	Rotunno and Emanuel (1987) model with capped warm rain and 'neutral' initial sounding.	As Experiment 7, but the 'neutral' sounding is used to initialize the far-field environment.

that the evolution of the vortex in this case is essentially unchanged from its capped counterpart.

The latest findings on the dependence of these exchange coefficients with wind speed (Black *et al.*, 2007) could be incorporated to further test our findings. However, in view of the uncertainties in the standard parametrizations employed for the planetary boundary layer, the subgrid-scale turbulence, and the cloud microphysical processes, these issues will be deferred for future work.

3. Warm-rain experiment

This section examines the warm-rain experiment (Experiment 1) focussing particular attention on the questions raised in the Introduction. Since the sea-to-air fluxes of latent and sensible heat are dependent on the local wind speed near the surface, we will adopt the maximum wind speed at any level as our primary vortex

coefficient exhibits a steady increase to a wind speed of approximately $25\,\mathrm{m\,s^{-1}}$ with correspondingly little systematic increase in the moisture exchange coefficient above $15\,\mathrm{m\,s^{-1}}$.

DOI: 10.1002/qj

intensification metric. The important effects brought about by the warm-rain process are highlighted by comparing these calculations with the pseudo-adiabatic experiment (Experiment 2) described in M1. Details of the warm-rain scheme as coded in MM5 can be found in Grell *et al.* (1995) and Hsie *et al.* (1984). In the scheme, the mixing ratios of water vapour, cloud water and rain water are predicted explicitly.

A summary of the vortex evolution is given in Figure 3, which shows time series of the maximum local wind speed ($VT_{\max}$) that occurs usually below the 1 km level, in association with one of the VHTs. As in the pseudo-adiabatic experiment, the vortex undergoes a similar gestation period that lasts approximately 9 hours; $VT_{\max}$ then increases quickly from 14.5 m s^{-1} to 27 m s^{-1} from 9 hours to 15 hours, and thereafter increases persistently to approximately 60 m s^{-1} at 68 hours.

It is clear that the intensification is delayed in the warm-rain experiment. We attribute this behaviour to a reduction in the convective instability that results from convectively driven downdraughts associated with the rain process (described further below) and due to the reduced buoyancy in clouds on account of water loading. These processes are believed also to limit the vortex intensity during the mature stage relative to the pseudo-adiabatic case. Nevertheless, during the intensification period, the activity of the VHTs (their merger and upscale growth as documented in M1) are qualitatively similar in both the warm-rain and pseudo-adiabatic experiments (not shown).

The primary difference between the warm-rain and pseudo-adiabatic experiment is that when rain droplets fall into unsaturated air, their evaporation moistens and cools the nearby air to approximately the wet-bulb temperature. The moist air tends to accelerate downwards as a result of the negative buoyancy caused by cooling of the air parcel and the water loading, which offsets adiabatic warming. Early into the intensification process, the precipitation-driven downdraughts act to significantly

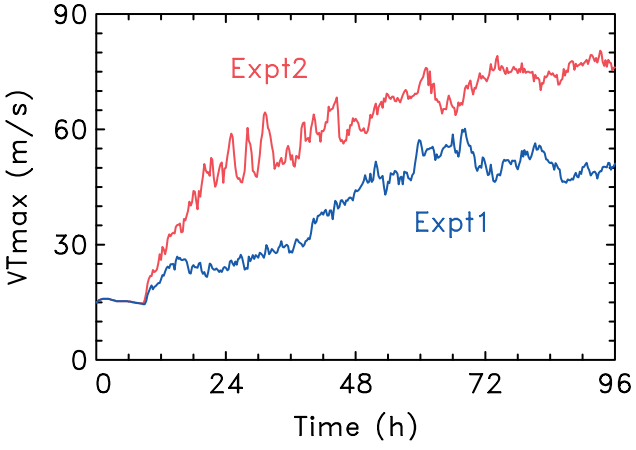

Figure 3. Time series of maximum total horizontal wind speed ($VT_{\max} = \max\sqrt{(u^2+v^2)}$) in Experiments 1 and 2. This maximum occurs mostly below an altitude of 1 km. This figure is available in colour online at www.interscience.wiley.com/journal/qj

reduce the θ_e in the boundary layer. Air parcels within these downdraughts carry their low θ_e air from middle and lower tropospheric levels into the boundary layer, creating local regions of low θ_e at the surface (Figure 4(a)). Those air parcels that reach the surface layer are slightly cooler than boundary-layer air parcels in the initial environment (not shown). Given the moisture replenishment from the surface fluxes, the local regions of low θ_e diminish in area as air parcels spiral in toward the vortex core. At later times (> 60 hours) there is still a broad region with depressed θ_e at the surface that extends outwards to approximately 200 km radius. However, a mesoscale region with locally enhanced θ_e eventually emerges near the centre (Figure 4(c)). At these later times, the θ_e deficit in the surrounding region has decreased to roughly 3–4 K, considerably smaller than the 15–20 K deficit found at earlier times in the intensification period (cf. Figure 4(a)). In other words, once the vortex reaches a quasi-steady state, the impact of precipitation-driven downdraughts is greatly reduced in the inner-core region as the winds are strong enough to maintain a sufficiently moist boundary layer. This feature has not been seen in the counterpart pseudo-adiabatic experiment at the corresponding time during intensification period with similar $V_{\max}$ (Figures 4(b) and (d)). Nevertheless, the key question remains: Is the intensification process controlled primarily by the WISHE mechanism?

An important first clue to answer this question is revealed in Figure 5, which shows the azimuthal-mean horizontal wind speed superimposed on the difference in azimuthal mean equivalent potential temperature θ_e from its initial value at three representative times (24, 48 and 60 hours) during the vortex intensification phase. The figure is constructed in analogy with Figure 4 of Rotunno and Emanuel (1987). Inspection of the plotted data shows that the *near-surface* wind speed increases without a concomitant increase in the mean surface θ_e in the vicinity of the radius of maximum wind speed. The increase in mean θ_e occurs outside the core. Furthermore, Figure 5 shows that the vortex intensifies without an enhanced negative radial gradient of azimuthal mean surface θ_e at the radius of maximum surface wind speed, the *sine qua non* of tropical cyclone intensification via WISHE as summarized in the Introduction. How, then, does the vortex intensify if it does not intensify by the WISHE mechanism?

3.1. Local buoyancy?

A second clue is revealed by examining whether the simulated VHTs during the intensification phase possess significant local buoyancy (Smith *et al.*, 2005). To do this we have calculated the deviation of the density temperature (T'_ρ) from its corresponding axisymmetric field at 5 km altitude for the warm-rain experiment at times when the system-scale vortex is amplifying. This azimuthally averaged density temperature serves as

DOI: 10.1002/qj

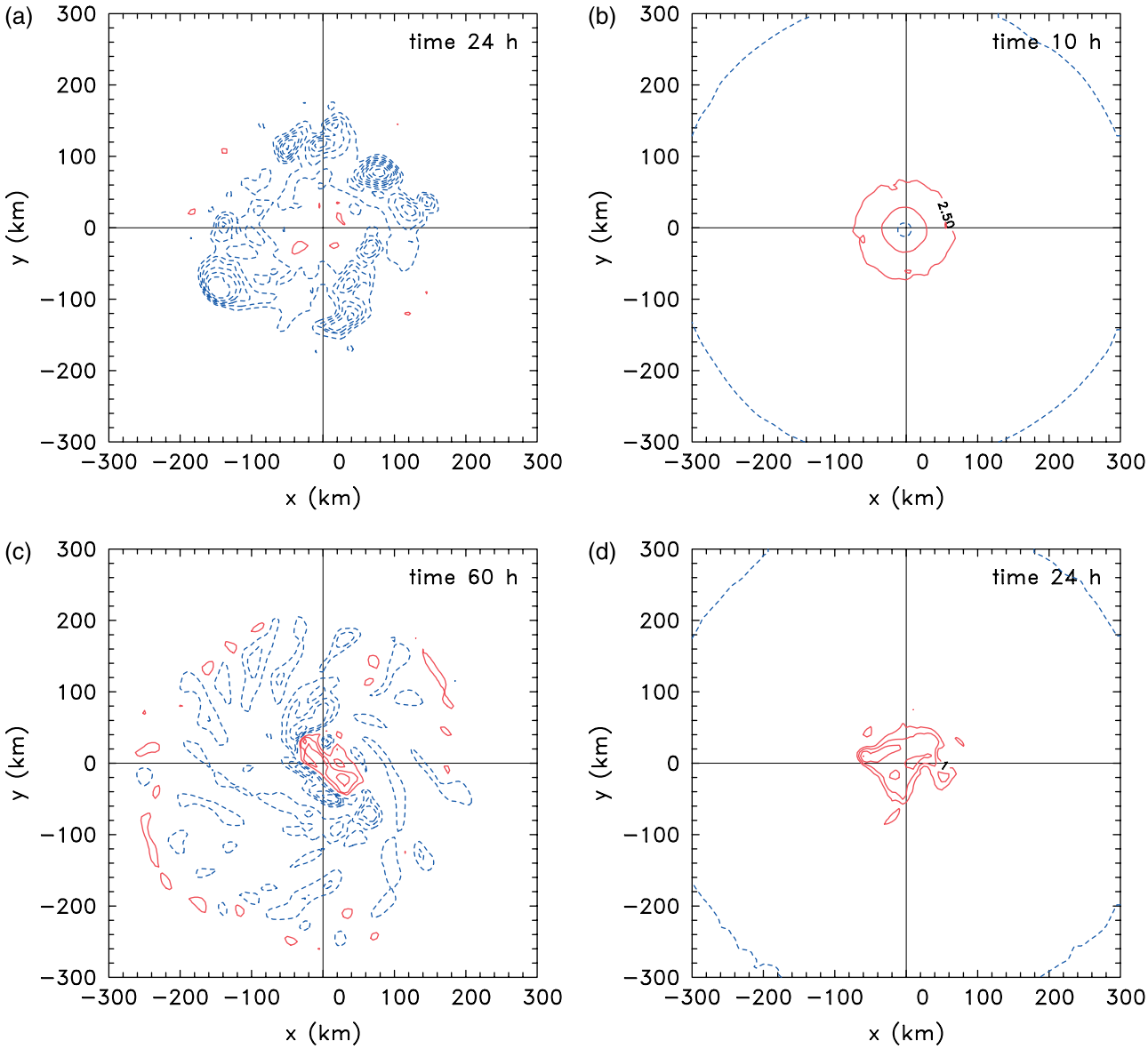

Figure 4. Horizontal cross-section of deviation of θ_e from a base value at the lowest model level (~ 40 m) as derived from the MM5 output (using Bolton, 1980) on the 5 km mesh domain for Experiment 1 at (a) 24 hours and (c) 60 hours, and Experiment 2 at (b) 10 hours and (d) 24 hours. The base value of θ_e is 360 K for (a), (b), 362 K for (c), and 361 K for (d). The contour interval is 2.5 K for (a, b), and 1 K for (c, d); dashed contours indicate negative values. This figure is available in colour online at www.interscience.wiley.com/journal/qj

the relevant reference environment for estimating the buoyancy in the VHTs.[§]

The density temperature, T_ρ, is defined in the usual way so as to represent the temperature that dry air would have to have to yield the same density as moist cloudy air (Betts and Bartlo, 1991; Emanuel, 1994). i.e.

$$T_\rho = T\frac{(1+r/\epsilon)}{(1+r_T)} \qquad (2)$$

where T denotes thermodynamic temperature, ϵ the ratio of the molecular weight of water to the mean molecular weight of dry air (equivalent to the ratio of dry and water-vapour gas constants), r the water vapour mixing ratio, $r_T = r + r_l$ the total mixing ratio (vapour plus cloud

[§]In Smith *et al.* (2005), the axisymmetric balanced temperature T_b was used to define the environment for the buoyancy calculations presented therein. During the intensification phase of the vortices simulated here, however, the azimuthal-mean temperature field $\overline{T}$ is found to be systematically less than T_b by a few degrees Celsius in the core of the vortex, which includes the eyewall region. This behaviour may be understood by recalling the generalized Rossby adjustment problem wherein a stably stratified circular vortex initially in gradient and hydrostatic balance is subject to an unbalanced perturbation. For horizontal perturbation scales that are much less than the local Rossby radius of deformation, the mass field will tend to adjust to the wind field. Here, the VHTs represent the unbalanced perturbations to the mean vortex and the local Rossby radius of deformation is on the order of 100 km (e.g. Hack and Schubert, 1986). Now, remembering that the adjustment time is typically on the order of several local inertial periods ($\pi/\overline{\Omega} \approx 2$ h, where $\overline{\Omega}$ is the azimuthal average angular velocity of the system vortex), we should not be surprised to find $\overline{T}$ systematically lagging behind T_b during the intensification phase. For this reason we suggest using the instantaneous azimuthal mean temperature $\overline{T}$ to define the local environment for the VHTs when calculating the parcel buoyancy of a VHT within an intensifying tropical cyclone.

DOI: 10.1002/qj

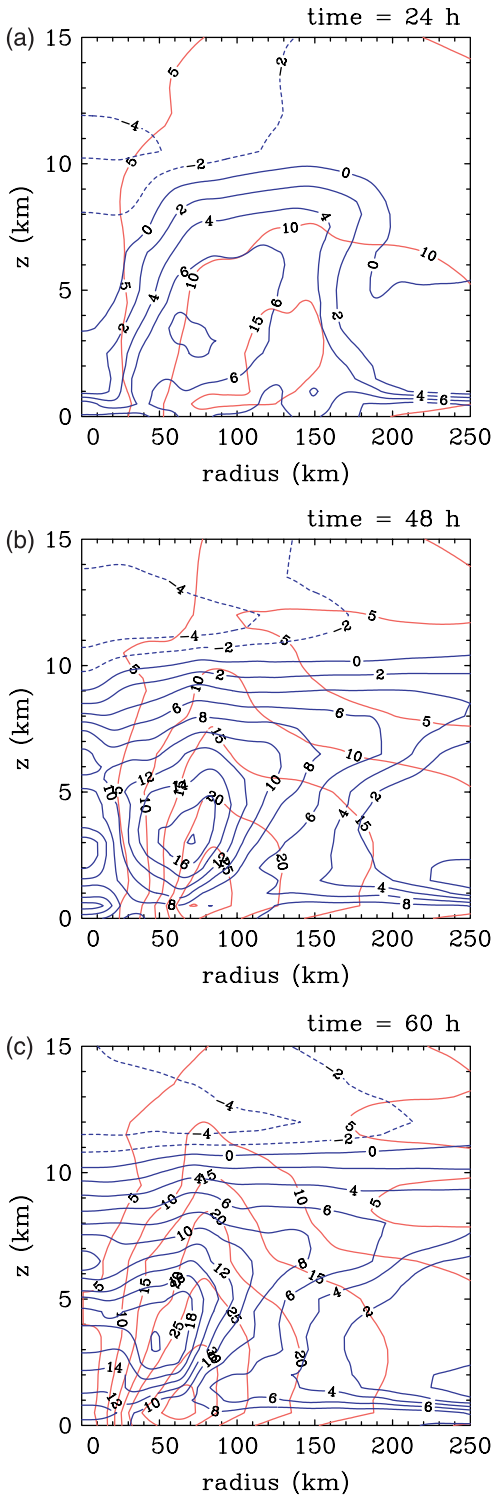

Figure 5. Radius–height cross-section of azimuthally averaged horizontal wind speed, $(u^2 + v^2)^{1/2}$, (contour interval 5 m s^{-1}) and θ_e deviation from the initial time (contour interval 2 K, negative values dashed) on the 5 km mesh domain for Experiment 1 at 24, 48, and 60 hours.

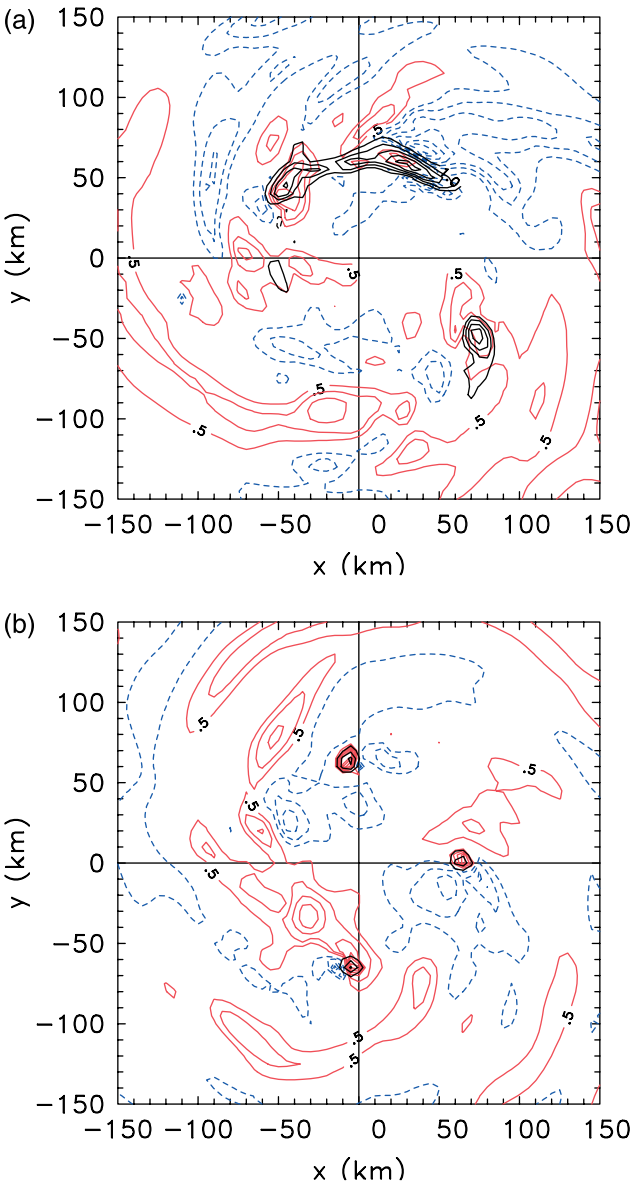

Figure 6. Horizontal cross-section at 5 km altitude of the deviation of density temperature from the azimuthal mean field for (a) Experiment 1 at 60 hours and (b) the corresponding virtual temperature deviation for Experiment 2 at 24 hours. Positive values of temperature deviation are denoted by solid contours and negative values by dashed contours; the contour interval is 0.5 K. The vertical velocity at the same level (black contours) is superimposed to corroborate the juxtaposition of regions of strong upward motion and local warmth. The contour interval is 1 m s^{-1} for (a) (warm rain) and 5 m s^{-1} for (b) (pseudo-adiabatic).

water), and r_l the cloud liquid water mixing ratio. In the absence of cloud water (as in the pseudo-adiabatic experiment), we have $r_l = 0$ and the density temperature reduces to the virtual temperature $T_v \approx T(1 + 0.608r)$.

In general, the local buoyancy in a region increases monotonically with T'_ρ. Figure 6(a) shows an example of the density temperature deviation and regions of strong upward motion at $z = 5$ km. Some regions with T'_ρ greater than 1 K in the warm-rain experiment are found to contain local regions of strong upward motion. The maximum value of T'_ρ is as large as 2 K in one of the active updraughts. As a point of reference, the maximum value of T'_v for the pseudo-adiabatic experiment (Figure 6(b)) at the same height and at a time with comparable VT_{max} is again approximately 2 K.¶

¶These findings have been confirmed at other times and are consistent with recent studies by Braun, (2002) and Saunders and Montgomery, (2004).

DOI: 10.1002/qj

The local buoyancy force per unit mass, b, acting within these model updraughts may be estimated as follows. Using the standard parcel approximation and neglecting water loading effects we use $b = gT'_v/T_v$. If, for simplicity, one approximates b as a constant over a 6 km depth between $z = 1$ km and $z = 7$ km, a back-of-the-envelope calculation assuming $T'_v/T_v = 1/300$ furnishes an updraught velocity of approximately 20 m s^{-1} at the 7 km level. Of course, this estimate neglects non-conservative processes and dynamic pressure effects near and within the updraught, both of which generally reduce the upward acceleration and hence reduce the updraught magnitudes (Houze, 1993).[‖]

The fact that the vertical velocity in these updraught cores increases with height over a deep stretch of the troposphere, in conjunction with the fact that these updraughts are co-located with intense vortical cores, suggests strongly that *latent instability is doing more than simply offsetting internal dissipation within the model's clouds* (cf. Emanuel, 1986; Rotunno and Emanuel, 1987). The local buoyancy (and latent instability) supports the generation of deep localized updraughts that act to stretch the pre-existing vertical vorticity, creating localized cores of intense cyclonic vorticity and warmth that are the dominant coherent structures during genesis and intensification (Montgomery *et al.*, 2006; M1).

3.2. Buoyancy source

It was shown in M1 that when the moisture flux was suppressed altogether there was no amplification of the system-scale winds and the initial CAPE was rapidly consumed (Figure 9 below). These findings imply that the source of local buoyancy in the VHTs during the intensification of the system-scale vortex does not come from the moist potential energy of the initial atmosphere. Rather, it must come from the underlying ocean.

To quantify the generation of local buoyancy in the VHT cores, we turn next to the diagnosis of the latent and sensible heat fluxes in both the warm-rain and pseudo-adiabatic experiments. Radial profiles of latent and sensible heat fluxes after azimuthally averaging around the circulation centre are shown in Figures 7(a) and (b) for the warm-rain and pseudo-adiabatic experiments, respectively. At 72 hours, the peak mean value of latent heat flux reaches approximately 480 W m^{-2} in the warm-rain experiment and 590 W m^{-2} in the pseudo-adiabatic experiment at 96 hours. For brevity, the sensible heat fluxes are not shown as their peak mean values are generally small compared with the latent heat fluxes, approximately 10% of the corresponding peak mean value of latent heat fluxes in both experiments. The radius of maximum latent heat fluxes coincides with the radius of maximum surface wind speed (RMW) and the maximum heat flux generally increases with VT_{max}. These latter features are

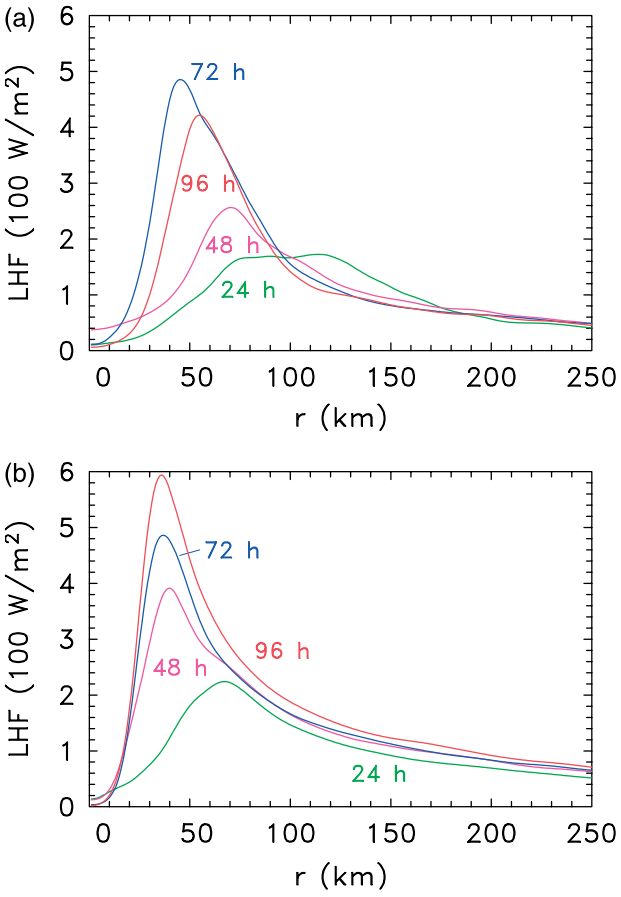

Figure 7. Radial profiles of azimuthally averaged latent heat flux diagnosed from the 5 km mesh domain for (a) Experiment 1 (warm rain) and (b) Experiment 2 (pseudo-adiabatic) at 24, 48, 72, 96 hours. This figure is available in colour online at www.interscience.wiley.com/journal/qj

hardly surprising in view of the fact that the bulk aerodynamic formulation mandates this behaviour by definition (assuming, of course, that the air–sea disequilibrium is approximately maintained). Furthermore, recalling the chain of processes indicated schematically in Figure 1, an increase of the fluxes with wind speed does not by itself prove that the intensification mechanism of the vortex as a whole occurs by the WISHE mechanism.

Figure 8 shows skew T–log p diagrams at four sample times during the intensification process (24, 36, 48, and 60 hours). Each figure depicts an azimuthal mean sounding at a particular radius of an active VHT (relative to the instantaneous centre of circulation defined by the vorticity centroid at 900 hPa) and a local vertical sounding through the core of this VHT. The horizontal coordinates of the VHT sounding are deduced from the coordinates of the maximum vertical velocity at the 5 km altitude. Consistent with the local buoyancy calculations presented above, Figures 8(a–d) indicate a non-trivial positive area between the moist adiabatic soundings rising through the VHTs and the local (axisymmetric) environment. As an example for Figure 8(b), the local CAPE of a hypothetical parcel lifted through a VHT relative to the axisymmetric mean sounding at the same radius is found to be approximately 350 J kg^{-1}. This is found to hold true for other times during the intensification process. These

[‖]During the intensification phase the maximum updraughts in the mid to upper troposphere are found to be in the range of 5–8 m s^{-1} and 10–15 m s^{-1}, in the warm-rain and pseudo-adiabatic experiments, respectively.

DOI: 10.1002/qj

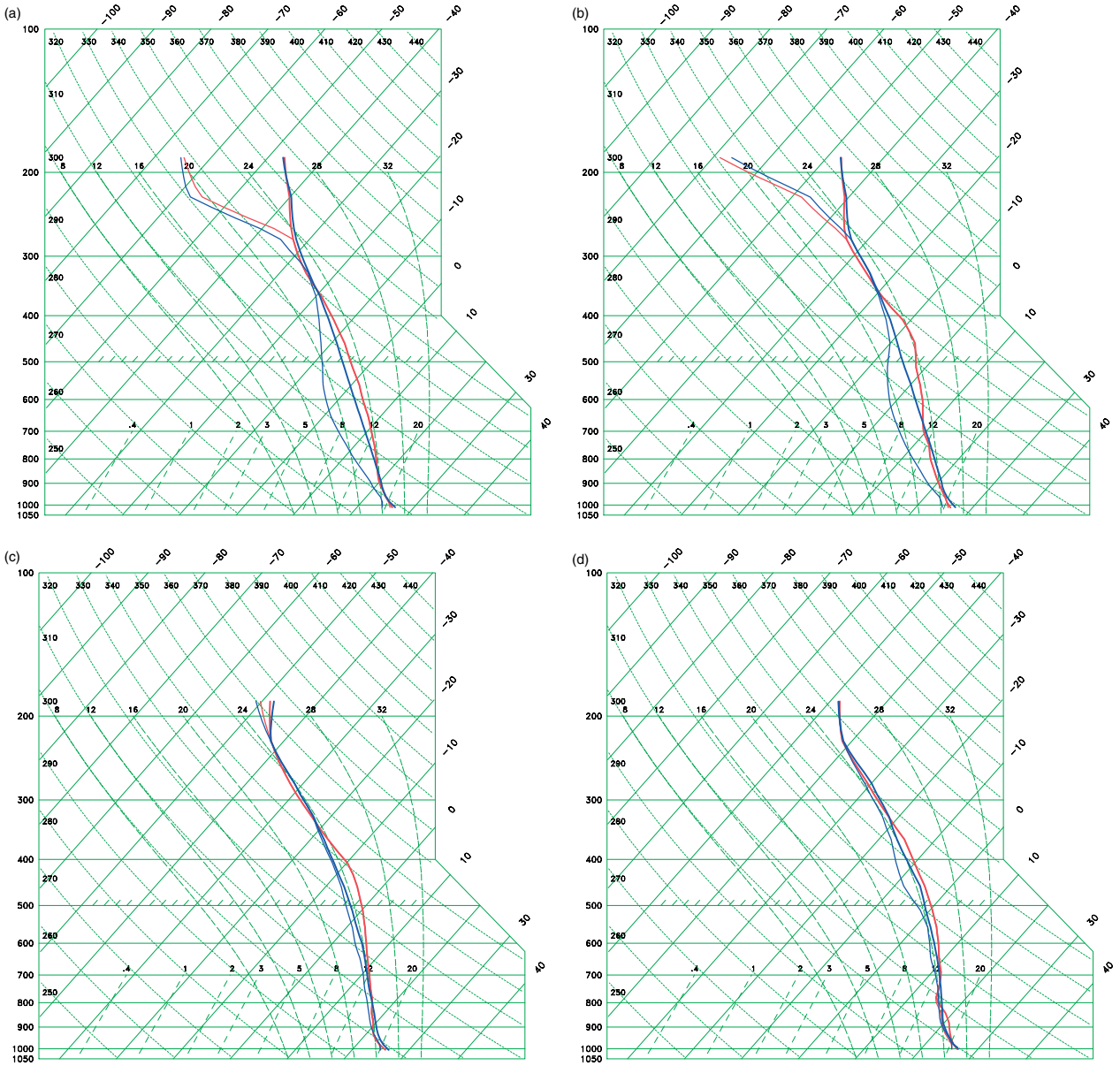

Figure 8. Vertical soundings as diagnosed from the 5 km mesh domain at 24, 36, 48, and 60 hours for Experiment 1 (warm rain). The red curve denotes a vertical sounding (temperature and dew point temperature) through an active VHT possessing the maximum upward velocity between 5 and 6 km altitude. The blue curves depict the azimuthal mean sounding at the particular radius of this active VHT. (See text for further details.)

results confirm the existence of positive local buoyancy to support accelerating updraughts and local vertical vortex-tube stretching (cf. Rotunno and Emanuel, 1987).

3.3. Summary

The evidence presented so far suggests a model of tropical cyclone intensification that is distinct from the WISHE mechanism presented in the Introduction. The vortex as a whole intensifies via buoyant VHTs generated by sea-to-air vapour fluxes until the system-scale vortex approaches a state in which its warm-core temperature structure tends to offset the *local* buoyancy liberated by the VHTs leading to a state of near convective neutrality. However, during the mature stage, VHTs continue to occur but are less numerous than during the intensification stage. Of course, when the vortex has reached maturity, near neutrality is to be interpreted along surfaces of azimuthal mean absolute angular momentum (Emanuel, 1986; Rotunno and Emanuel, 1987).

In the next two sections, we investigate this hypothesis further by suppressing the wind-speed dependence of the fluxes of latent and sensible heat above nominal trade-wind values.

4. Vortex evolution with capped fluxes

In M1 we investigated the evolution of the vortex when the dependence of wind speed in the bulk-aerodynamic formulae for latent- and sensible-heat fluxes was capped at $10\,\mathrm{m\,s^{-1}}$ (Experiment 4 in Table II). This wind-speed cap gives sea-to-air water vapour fluxes that never exceed $130\,\mathrm{W\,m^{-2}}$ (Figure 10 below), a value

DOI: 10.1002/qj

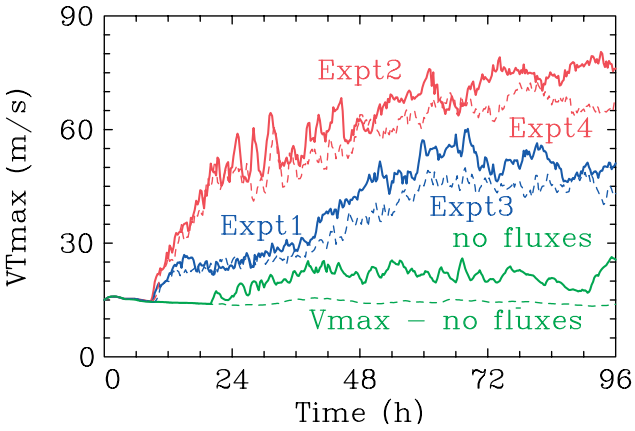

Figure 9. Time series of VT_{max} for Experiments 1–4. Also shown for reference is the time series of VT_{max} and azimuthally averaged tangential wind V_{max} of the experiment when the surface latent- and sensible-heat fluxes are set to zero (Experiment S3; Table II of M1).

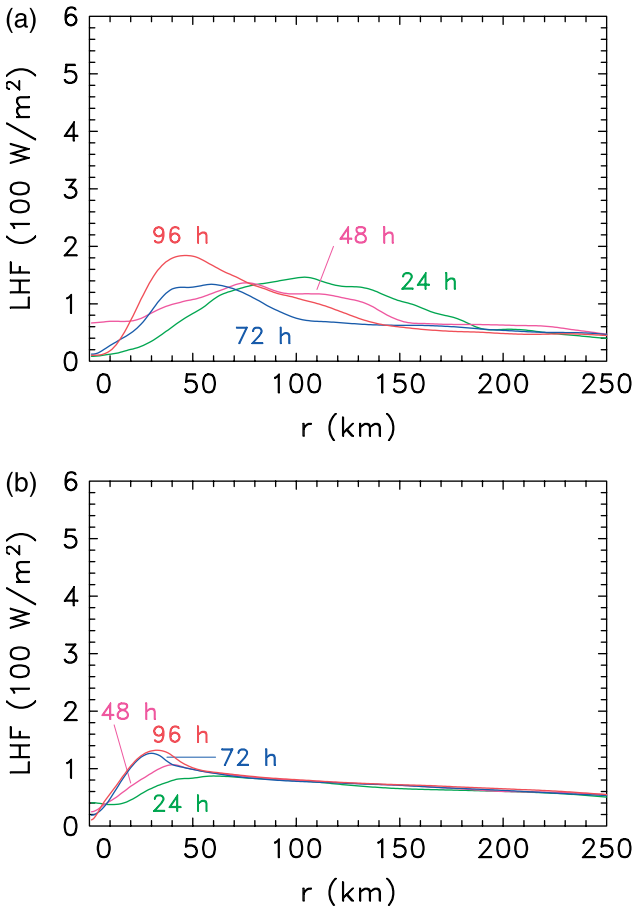

Figure 10. Radial profiles of azimuthally averaged latent heat flux as diagnosed from the 5 km mesh domain for (a) Experiment 3 (capped warm rain) and (b) Experiment 4 (capped pseudo-adiabatic) at 24, 48, 72, 96 hours. This figure is available in colour online at www.interscience.wiley.com/journal/qj

comparable to observed trade-wind values in the summer-hemisphere. It was found in M1 that under such a constraint, the characteristics of the vortex evolution did not change qualitatively compared to the pseudo-adiabatic experiment. A minimum value of approximately 3 m s^{-1} was found necessary for the wind-speed cap at which the vortex can still intensify to hurricane strength under the pseudo-adiabatic set-up of Experiment 4 (not shown).

The foregoing section suggested an intensification mechanism whose basic elements are the VHTs that obtain their local buoyancy from sea-to-air fluxes of water vapour. In this model, the vortex should continue to intensify until it reaches a state in which its warm-core temperature structure diminishes the local buoyancy liberated by the VHTs to a state of near neutrality along surfaces of mean absolute angular momentum. We show now that the warm-rain results are not fundamentally altered when the fluxes of latent and sensible heat are not allowed to increase with wind speed beyond approximately trade-wind values.

4.1. Warm-rain experiment with capped fluxes

Figure 9 shows the time series of VT_{max} in the capped warm-rain experiment (Experiment 3) and its uncapped counterpart (Experiment 1).** In the capped experiment, VT_{max} is generally smaller than in the uncapped experiment; the difference between the two never exceeds 15 m s^{-1}. The gestation period in the capped experiment is approximately 10 hours, only 1 hour longer than in the uncapped experiment and the intensification period has about the same duration (approximately two and a half days).

The radial distribution of the azimuthally averaged surface latent heat fluxes from the capped flux versions of the warm-rain and pseudo-adiabatic experiments are presented in Figure 10. The maximum latent heat flux is located near the instantaneous radius of maximum surface wind speed, even though the surface wind speed in the heat fluxes are capped at 10 m s^{-1}. In the capped warm-rain experiment, the heat flux increases from approximately 145 W m^{-2} at 24 hours to 185 W m^{-2} at 96 hours; in the capped pseudo-adiabatic experiment, the latent heat flux increases from approximately 90 W m^{-2} at 24 hours to 135 W m^{-2} at 96 hours. The latent heat flux in the capped warm-rain experiment is generally larger than in the capped pseudo-adiabatic experiment because the precipitation-driven downdraughts import low-θ_e air into the boundary layer, creating negative θ_e anomalies that have no counterpart in the capped pseudo-adiabatic run. The resulting drier air in the boundary layer increases the thermodynamic disequilibrium between ocean and atmosphere, which, in turn, increases the latent heat flux.

**In the pseudo-adiabatic experiment wherein the latent and sensible heat fluxes are suppressed altogether, we found that the system-scale vortex does not intensify, even though there is some transient hot-tower convection and local wind-speed enhancement. The result is plotted in Figure 9 for reference (Experiment S3 in M1 provides details). Despite the non-zero convective available potential energy present in the initial sounding, no system-scale wind amplification is observed. This rules out the possibility that vortex intensification with capped fluxes examined here is an artifact of using an initially unstable moist atmosphere (cf. Rotunno and Emanuel, 1987). Prompted by one of the reviewer's comments, we take up this issue again in the Appendix where we verify our main conclusions and interpretations using an initially neutral sounding.

DOI: 10.1002/qj

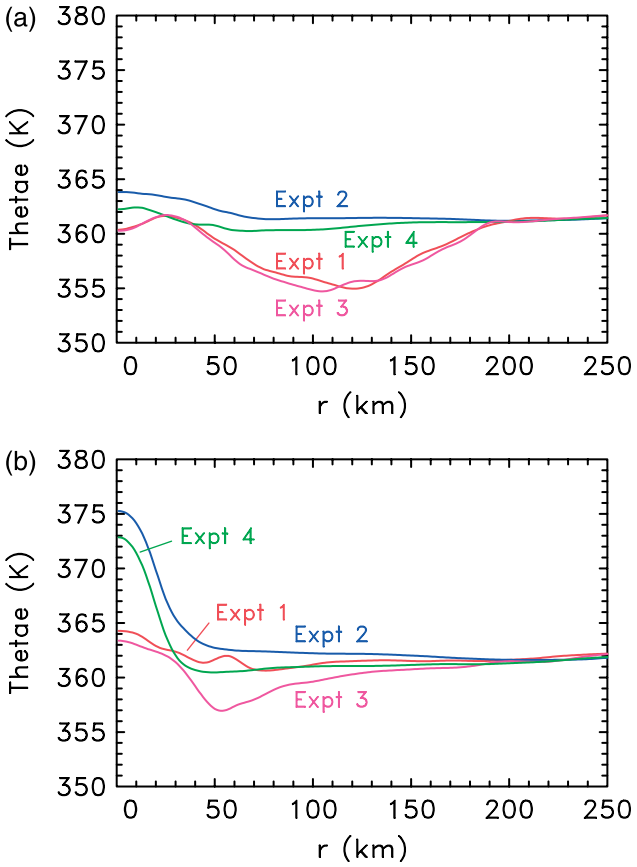

Figure 11. Azimuthal mean of θ_e at the lowest model level (~ 40 m) at (a) 24 hours and (b) 60 hours of Experiments 1–4. This figure is available in colour online at www.interscience.wiley.com/journal/qj

For similar reasons, the local θ_e deficits in the capped warm-rain experiment are somewhat larger in magnitude than in the corresponding warm-rain experiment. This is because, in the capped experiment, the fluxes from ocean are limited in their ability to offset the evaporative-cooling effects. Figure 11 illustrates this point at 24 and 60 hours. At 24 hours the azimuthal mean surface θ_e for both experiments is similar in shape and magnitude near 110 km radius. By 60 hours the mean surface θ_e deficit has been largely eradicated in the capped experiment, but the values are still depressed relative to the uncapped run by as much as 5 K near the radius of maximum wind speed near 50 km radius. Inwards of 50 km, however, the mean surface θ_e in the capped experiment increases rapidly with decreasing radius and comes within 0.5 K from its uncapped counterpart inside the model eye.

Despite these quantitative differences, it is clear that VT_{max} increases similarly with time during the intensification phase for both warm-rain and capped warm-rain experiments. This supports the hypothesis proposed in section 3 that the basic intensification process in the cloud model is not essentially dependent on the WISHE mechanism.

4.2. Discussion and interpretation

With the inclusion of precipitation and evaporative processes, precipitation-driven downdraughts import cool and dry air into the boundary layer, yielding local surface θ_e deficits relative to the exterior region of the vortex. Despite the limited replenishment by latent and sensible heat fluxes in the capped experiments, the local θ_e deficit for inflowing parcels is still reduced by non-zero but persistent sea-to-air moisture fluxes. This behaviour can be understood using a simple slab boundary-layer model in the limit of steady and nearly axisymmetric flow. Here, the advection of boundary-layer θ_e along a curved streamline is balanced by the sum of surface heat fluxes from the underlying ocean and the entrainment of θ_e from above the boundary layer by a combination of vortex-scale subsidence and turbulent (primarily convective) fluxes. Radiative cooling is again neglected for simplicity.

A lower-bound estimate for the characteristic recovery length-scale and the recovery time-scale of θ_e for inward-moving parcels may be obtained upon solving the equation for θ_e in the boundary layer in the region outside the core in the limit of vanishing downward advection by mean subsidence and turbulent (convective) processes. At first, we consider the uncapped flux limit. The circumferential recovery length-scale is found to be $h\alpha/C_k$ and the recovery time-scale is $h\alpha/C_kV$, where h denotes the mean boundary-layer depth, α a reduction factor relating the near-surface wind to the depth-averaged boundary-layer wind speed V, and C_k the enthalpy exchange coefficient governing the rate of moist entropy flux from sea to air (Emanuel, 1995). As noted in section 2, the value of C_k does not vary appreciably for the bulk-aerodynamic boundary-layer scheme in MM5 and the effects of the variation of C_k on the vortex evolution is negligible compared to the case when C_k is constant (see result of Experiment 11 in section 5).

Based on our model data, we take $h = 1$ km, $C_k = 1.29 \times 10^{-3}$, and $\alpha = 0.9$. Since the horizontal wind speed early into the intensification process is not far above the initial wind speed maximum, we take $V = 20\,\mathrm{m\,s^{-1}}$. The circumferential recovery length-scale is about 700 km and the recovery time-scale is about 10 hours. Capping of the horizontal wind speed in the surface fluxes would obviously increase the recovery length- and time-scales somewhat. Considering the results presented in section 3 and the drastic assumptions invoked here, these values appear to be reasonable lower-bound estimates. This is because the θ_e recovery is persistently frustrated by the downward import of low θ_e into the boundary layer from convective downdraughts and vortex-scale subsidence.

Whereas a persistent, but weak, vortex-scale subsidence into the boundary layer outside the core is present in our model solutions (not shown), neither this process nor the convective downdraughts are strong enough to obstruct the slow, but persistent recovery en route. Therefore, even with capped surface fluxes at nominal trade-wind values, the boundary-layer recovery is still adequate to supply the VHTs with sufficient local buoyancy relative to their local environment, and consequently the vortex as a whole is able to amplify almost as rapidly as in the uncapped experiments.

DOI: 10.1002/qj

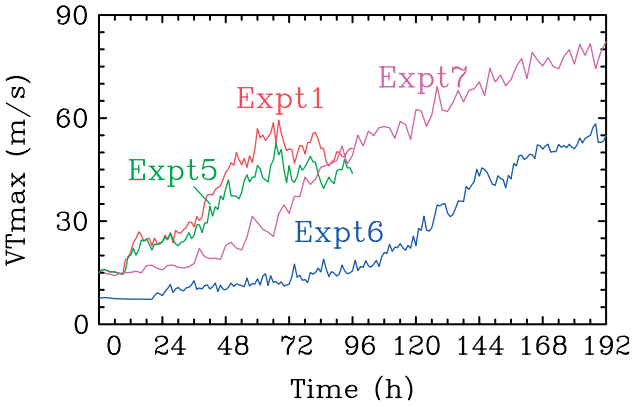

Figure 12. Time series of VT_{max} for Experiments 1 and 5–7. Table II gives details of these experiments. This figure is available in colour online at www.interscience.wiley.com/journal/qj

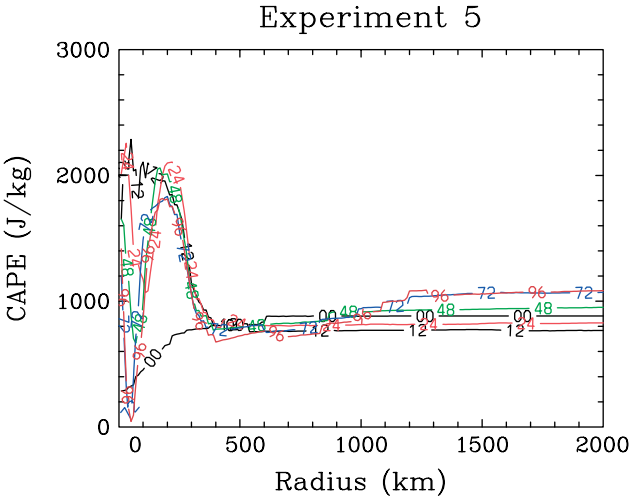

Figure 13. Radial profiles of surface-based CAPE for Experiment 5, averaged azimuthally around the storm centre at 0, 12, 24, 48, 72 and 96 hours. This figure is available in colour online at www.interscience.wiley.com/journal/qj

On the basis of the foregoing results, we suggest that WISHE is not the essential nor the dominant mechanism of tropical cyclone intensification (cf. Carrier *et al.*, 1971). *As emphasized in M1, non-trivial, but modest sea-to-air vapour fluxes are essential; the wind–evaporation feedback process is not.*

5. Three sensitivity experiments

We discuss now three sensitivity experiments, Experiments 5–7 (Table II) that are designed to further test the hypothesis that the wind–evaporation feedback process is not essential for tropical cyclone intensification. (Additional sensitivity Experiments (8–14) are presented in the Appendix.) Figure 12 summarizes the time series of VT_{max} obtained from these experiments, together with that for the warm-rain experiment (Experiment 1, described in section 3), which is included for reference. Only the principal results as they relate to the main hypothesis are recorded here.

5.1. Capped relative humidity in the environment

Experiments 5 and 6 are conducted to test the influence of environmental near-surface relative humidity on the intensification process. Recall that shallow convective processes and spiral rainbands generally play an important role in the moisture and hence equivalent potential temperature budgets of the hurricane boundary layer outside the high-wind region of the storm (Barnes *et al.*, 1983; Powell, 1990; Emanuel, 1986, 1995; Ooyama, 1997; Smith, 2003; Smith and Vogl, 2008). However, at the spatial resolutions employed here, these processes are not well represented, if at all, in the MM5 model. To accurately represent these processes, large-eddy simulations are probably necessary – requiring a horizontal grid spacing on the order of 100 m! For the bulk-aerodynamic boundary-layer parametrization used in the MM5 model, a simple K-theory closure for the vertical turbulent fluxes in the boundary layer serves as the surrogate for shallow convection. More sophisticated boundary-layer closure models lie outside the scope of the current work.

In Experiment 5 the relative humidity at the lowest model level (approximately 40 m height) is capped at 80% for the two outer domains (45 and 15 km grid mesh). This procedure prevents the environment from moistening artificially and supplying the inner region with an enhanced reservoir of CAPE.[††] The evolution of VT_{max} is generally the same as in the standard warm-rain experiments (Experiments 1, 3) during the simulation time (96 hours). Figure 13 displays the surface-based CAPE averaged azimuthally around the storm centre as a function of radius at 0, 12, 24, 48, 72 and 96 hours. It is evident that CAPE in the far environment does not increase substantially (on the order of 300 J kg^{-1}) during the four-day integration. At smaller radii ($250 < r < 1250$ km), CAPE decreases somewhat due to a slight warming in the mid- to upper-troposphere associated with the latent heat release in the core region and the advection of this warm air by the outflow circulation in the upper troposphere. Not surprisingly, near the core, where the surface RH is no longer capped, the boundary layer moistens even with the modest capped wind and the CAPE markedly increases.

Although capping the near-surface relative humidity is a crude expedient for mimicking shallow convection in the vortex environment, this experiment allays the concern that the vortex intensification is an artifice of tapping the environmental reservoir of heightened convective instability, rather than generating convective instability locally by surface fluxes in the region with non-trivial wind speeds. This matter is taken up again in the Appendix using an initially moist neutral sounding.

[††] Assuming, as is the case here, that the ambient sounding is not drier at a height of 40 m.

DOI: 10.1002/qj

5.2. Capped relative humidity, weaker initial vortex

Experiment 6 differs from Experiment 5 in two respects: (i) the initial $VT_{\max}$ is reduced to $7.5\,\mathrm{m\,s^{-1}}$ instead of $15\,\mathrm{m\,s^{-1}}$, and (ii) the near-surface wind-speed cap is reduced to $7.5\,\mathrm{m\,s^{-1}}$ for latent and sensible heat fluxes. Again, the relative humidity at the lowest model level is capped at 80% outside of domain three for reasons already articulated. It is evident that the evolution of $VT_{\max}$ approaches that of the counterpart Experiment 5, but the period of most rapid intensification is delayed significantly. The results support the hypothesis that the WISHE intensification mechanism is not essential even for a weak tropical-depression-strength vortex, but that the VHT pathway for intensification is effective.

5.3. An axisymmetric calculation

The axisymmetric experiment, Experiment 7, departs from our three-dimensional theme, but it is a useful benchmark since the WISHE model was developed using axisymmetric reasoning and modelling. This experiment allows also a preliminary quantitative comparison of the axisymmetric and non-axisymmetric spin-up timescales. The Rotunno and Emanuel (1987) model is used here (courtesy of R. Rotunno, personal communication). The basic parameters are the same as in the companion Experiment 3 above, including a sea surface temperature of 27 °C, an initial vortex with identical tangential velocity distribution below $z = 18\,\mathrm{km}$ altitude, the same Coriolis parameter and initial sounding.

The radial grid spacing is 3 km (somewhat smaller than the corresponding horizontal grid increment employed in Experiment 3) and the vertical grid spacing is 312.5 m. The surface wind speed in the latent and sensible heat fluxes is capped at $10\,\mathrm{m\,s^{-1}}$ and the bulk-aerodynamic transfer coefficients for heat and momentum are set to constant values of 1.3×10^{-3} and 1.01×10^{-3}, respectively. These values correspond approximately to the mean values of these coefficients as diagnosed from the off-the-shelf MM5 bulk-aerodynamic boundary-layer scheme in the unstable boundary-layer regime. Radiative cooling is again neglected to be consistent with the MM5 experiments presented earlier.

Figure 12 shows clearly that the model vortex intensifies, albeit slowly, to a minimal hurricane vortex by approximately 72 hours. Interestingly, the intensification rate at early times is noticeably smaller than the corresponding capped warm-rain experiment in the three-dimensional model (Experiment 3). On the other hand, the intensity at longer times is significantly stronger than in the three-dimensional model. The reason for the lethargic development at early times and the stronger intensity at later times is not yet clear to us, but we can speculate on several likely factors including differences between locally buoyant VHTs and convective rings in axisymmetric geometry, differences in the corresponding downdraught phenomenology of these convective structures, differences in the spatial and temporal accuracy of the two models, and differences in the warm-rain microphysics that in turn regulate the strength of convective downdraughts. It should be noted that in the axisymmetric model the rate of intensification and the mature intensity are significantly larger when the fluxes are not capped, unlike the three-dimensional case (Appendix). A more complete understanding of the differences between rotating moist fluid dynamics in axisymmetric and three-dimensional geometries appears to be an interesting topic for further research.

These issues notwithstanding, the outcome of Experiment 7 is clear: even in an axisymmetric configuration, tropical cyclone intensification does not hinge on the evaporation–wind feedback mechanism known as WISHE as previously suggested (Emanuel *et al.*, 1994; Craig and Gray, 1996; Gray and Craig, 1998; Emanuel, 2003).

6. Conclusions

In this paper we have sought and obtained a deeper understanding of tropical cyclone intensification in three dimensions when precipitation and evaporative-cooling (warm-rain) processes are included. Consistent with our findings presented in M1, intensification with warm-rain physics is again dominated by VHTs. The results point to an intensification pathway wherein the VHTs are the coherent structures that ultimately result in the spin-up of the system-scale vortex. The VHT pathway is distinct from the purely thermodynamic model associated with the evaporation–wind feedback mechanism articulated in the Introduction, which has become the accepted paradigm of tropical cyclone intensification in textbooks and recent literature. A positive feedback between the azimuthal-mean boundary-layer equivalent potential temperature and the azimuthal-mean surface wind speed underneath the eyewall of the storm is shown to be unnecessary in both three-dimensional and axisymmetric configurations that limit the surface wind speed in the sea-to-air vapour fluxes at a nominal (trade-wind) value, thereby excising the wind-evaporation mechanism in the model. The Appendix considers some additional sensitivity experiments examining the influence of using an initially neutral sounding and other model and physics configurations. The outcome is that, even without heat fluxes in the vortex environment and using velocity-limited heat fluxes ($10\,\mathrm{m\,s^{-1}}$) in the vortex region, the evaporation–wind intensification mechanism known as WISHE is subdominant compared to the VHT intensification mechanism.

The intensification mechanism in three dimensions is via the generation of locally buoyant VHTs and the near-surface convergence that the VHTs induce within the boundary layer. During the amplification process we find that the system-scale density temperature generally lags behind the local density temperature within the VHT cores. It is these cores that drive the intensification process until the system-scale temperature along absolute angular momentum surfaces nearly coincides with the

DOI: 10.1002/qj

local temperature of the VHT cores. Our companion paper M3 provides a more in-depth analysis and a new perspective on the axisymmetric aspects of the spin-up process.

The current findings refute the prevailing view that tropical cyclones are premier examples of vortical systems arising from evaporation–wind feedback known as WISHE. Given the potential significance to our understanding of the dynamics of hurricanes, and given the limitations of the present modelling framework, further tests of these predictions are advocated using data collected by National Oceanic and Atmospheric Administration and United States Air Force aircraft during observed intensification episodes of tropical cyclones. A recent observational analysis reported by Molinari *et al.* (2004; their Figure 12) supports the hypothesis advanced here, but a more comprehensive survey of intensifying storms is required.

Acknowledgements

This basic research on tropical cyclones was supported in part by the Office of Naval Research grant N001408WR20129, by National Science Foundation grants ATM-0649944, ATM-0649946, ATM-0715426, NOAA grant 2007-AOML-E8R2H and by a grant from the German Research Council (DFG). The work was initiated between daily planning meetings and research flights while in the field on Guam, and was soon after completed at NOAA's Hurricane Research Division (HRD) and the Naval Postgraduate School (NPS). We would like to thank the ONR/NSF-supported scientists (especially Pat Harr, Russ Elsberry of the NPS and Peter Black of NRL/Monterey), the professional and student forecasters, the flight crews and support personnel who worked tirelessly to make the field campaign a success. The science team fostered a stimulating atmosphere for conducting tropical cyclone research. Finally, we thank NOAA-HRD for their generous hospitality and both HRD and NPS for creating a stimulating environment for pursuing hurricane research. We thank the two reviewers, Kerry Emanuel and Suzanne Gray, for their perceptive comments on the original version of our paper. The second author is grateful for travel support provided by the DFG as part of the project 'Improved quantitative precipitation forecasting in Vietnam'.

Appendix

Additional sensitivity experiments

Here we report briefly on a further set of sensitivity experiments, Experiments 8–14 in Table II. The time series of VT_{max} obtained from these experiments, together with that for the warm-rain experiment, Experiment 1, are shown in Figures A.1 and A.3. These experiments are conducted to assess the robustness of our conclusions in the main text to several additional physical effects and model configurations. A detailed description and salient results are provided below.

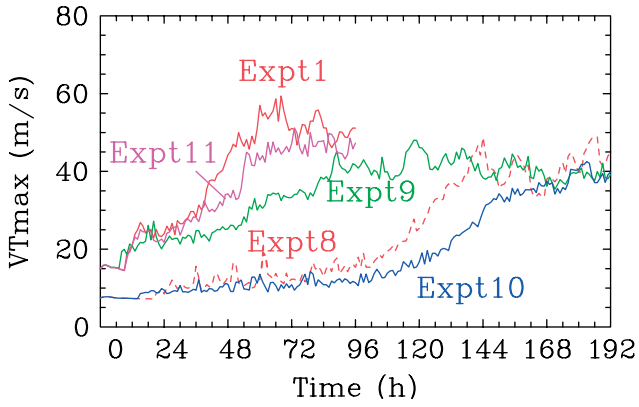

Figure A.1. Time series of VT_{max} for Experiments 1 and 8–11. Table II povides details of these experiments. This figure is available in colour online at www.interscience.wiley.com/journal/qj

A.1. Experiment 8: Weaker initial vortex

In Experiment 8, the initial VT_{max} is reduced to 7.5 m s^{-1} and the wind speed in the surface heat fluxes is capped at 7.5 m s^{-1}. In this case, VT_{max} increases slowly from 9 m s^{-1} at 21 hours to 15 m s^{-1} at 96 hours. A rapid intensification phase then ensues until 141 hours at which time VT_{max} reaches 49 m s^{-1}. Subsequently, the intensity fluctuates around 45 m s^{-1}. Thus, for the standard choice of MM5 parameters used here, halving the initial vortex amplitude does not nullify the intensification process. This suggests that the WISHE intensification mechanism is not essential, even when starting from a weak tropical-depression-strength vortex.

A.2. Experiments 9 and 10: Higher horizontal resolution

In Experiment 9 we use the capped warm-rain configuration of Experiment 3, but add a fourth domain (300 km square) with a horizontal grid spacing of 1.67 km. The surface wind speed cap in the latent and sensible heat fluxes is set to 10 m s^{-1}. After a slightly reduced gestation period, the vortex intensifies slowly to 43 m s^{-1} at 96 hours and the intensity fluctuates around 40 m s^{-1} until 192 hours. The higher horizontal resolution delays the onset of rapid intensification. Whereas the resulting vortex exhibits a slightly lower intensity than found in Experiment 3 (due in part to more vigorous and widespread downdraught activity relative to the coarser resolution experiment – not shown), the increased resolution impedes, but does not obstruct the intensification process in the absence of the WISHE mechanism.

Experiment 10 is the same as Experiment 8 (a weak initial vortex with VT_{max} = 7.5 m s^{-1} and a wind speed cap of 7.5 m s^{-1} in the surface heat fluxes), but has a fourth domain (300 km square) with a horizontal grid spacing of 1.67 km. As in Experiment 5, the higher horizontal resolution delays the onset of rapid intensification. Again, this feature is attributed primarily to the more vigorous and widespread downdraught activity, which tends to enhance the import of low θ_e into the boundary layer relative to the coarser resolution counterpart. We note briefly here that this behaviour is quite unlike that found in axisymmetric

DOI: 10.1002/qj

hurricane models in which increases in spatial resolution (with a standard eddy diffusivity that decreases with increasing resolution) yield consistently stronger storms until model convergence (e.g. Persing and Montgomery, 2003). This discrepancy between three-dimensional and axisymmetric behaviour is interesting (see discussion of Experiment 7 in the main text for more).

A.3. Experiment 11: Bulk aerodynamic scheme in MM5

As mentioned in section 2, in the bulk-aerodynamic scheme as coded in MM5, the heat and momentum exchange coefficients are spatially variable even in the 'capped flux' configuration because of the variation induced by the stability factor in the bulk Richardson number. For example, an examination of Experiment 3 shows that, during the intensification period, the region of unstable points ($Ri_B < 0$) is located within approximately 100 km radius from the vortex centre. There are two distinct branches of values for C_k corresponding to the stable/unstable condition. The value of C_k for the unstable points are generally 20% greater and more variable than that of the stable points (not shown). To establish the robustness of our conclusions obtained with the 'capped' experiments, we perform an experiment (Experiment 11) with the same configuration as Experiment 5, except that the bulk-aerodynamic scheme used in the model is modified so that C_k is held constant at 1.3×10^{-3} for all three domains. From the resulting time series for VT_{max} shown in Figures 12 and A.1, we clearly see that the evolution in Experiments 5 and 11 is generally similar. This result supports further the general conclusion that the evaporation–wind feedback process as articulated in the Introduction is not essential for tropical cyclone intensification.

A.4. Experiments 12 and 13: A 'neutral' initial sounding and doubly periodic boundary conditions, uncapped heat fluxes (Experiment 12) versus capped heat fluxes on a fine grid within a circular region of 300 km radius and zero fluxes elsewhere (Experiment 13)

In Experiment 12, the far-field environment is initialized with the so-called 'neutral' initial sounding from the Rotunno and Emanuel (1987) model (Figure A.2). This sounding was generated by running the RE87 model with an initially quiescent Jordan sounding environment to a state of near-convective equilibrium.[‡‡]

In addition, a simple radiative-cooling scheme has been employed that relaxes the temperature at every grid point to the initial sounding with a cooling time-scale of one day. Finally, the MM5 model is modified to have periodic boundary conditions on the coarsest domain in both north–south and east–west directions. Experiment 12 is otherwise the same as Experiment 1.

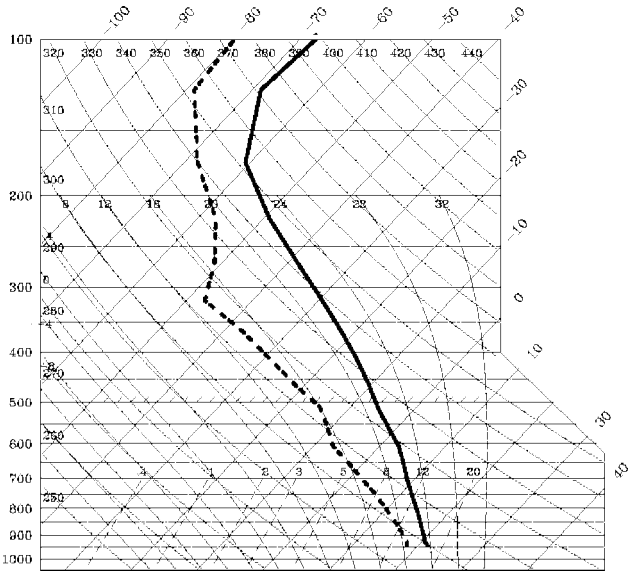

Figure A.2. Skew $T-\log p$ diagram showing the temperature (solid line) and dew point (dashed line) of a 'neutral' sounding from the Rotunno and Emanuel (1987) model. This sounding is used to initialize the far-field environment in Experiments 12–14.

As detailed in Table II, the configuration of Experiment 13 is the same as in Experiment 12, except that the wind speed dependence of surface heat fluxes is capped at $10\,m\,s^{-1}$ within a circular region of 300 km radius from the domain centre on the fine grid (5 km mesh) and surface heat fluxes are set to zero elsewhere. This experiment is a stringent test of our hypothesis since it leaves no possibility for the contribution of environmental CAPE on the intensification process.

The results of Experiments 12 and 13 will be discussed in the next subsection in comparison to Experiment 14 using an axisymmetric model.

A.5. Experiment 14: A 'neutral' sounding and capped heat fluxes in an axisymmetric model

The configuration of Experiment 14 is the same as Experiment 7, except that the 'neutral' sounding is used to initialize the far-field environment. No radiative cooling is used in this case. Since the horizontal grid spacing is uniform in the Rotunno and Emanuel model, a 3 km radial grid spacing renders the model atmosphere 'convection permitting' throughout the domain. This experiment thus has the added value of testing whether our results in the main text are an artifact of the coarse resolution of the MM5 model in the outer domain and the corresponding tendency for deep convection to be suppressed there and the concomitant spurious build-up of ambient CAPE.

Figure A.3 shows time series of VT_{max} for Experiments 12, 13 and 14. Experiment 1 is shown for reference. For all three sensitivity experiments, the vortex intensifies to hurricane strength after 96 hours. The vortex intensity

[‡‡]Of course we are fully aware of the fact that a neutral sounding in one model is not necessarily neutral in another, given the dependence of convective instability in a discrete model to model physics, to resolution, and even to dimensionality. For a hypothetical air parcel lifted from the lowest model level, the CAPE is approximately $100\,J\,kg^{-1}$; this is considerably smaller than approximately $900\,J\,kg^{-1}$ for the approximate Jordan sounding used in Experiments 1–7. The very small CAPE is thought to be sufficient to balance internal dissipation within the model's clouds and for this reason the sounding is considered 'neutral'.

DOI: 10.1002/qj

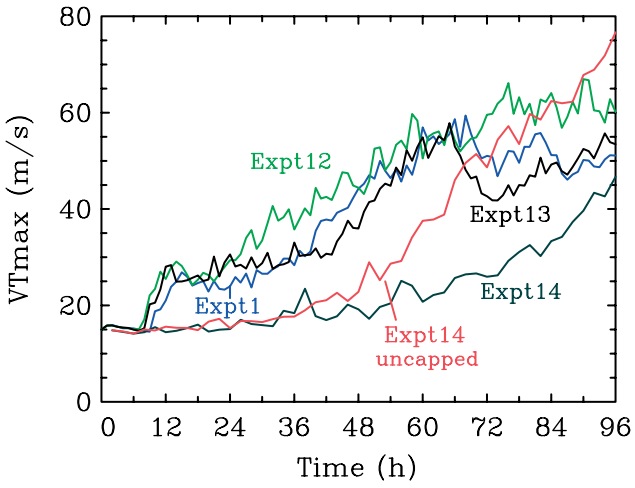

Figure A.3. Time series of VT_{max} through to 4 days for Experiments 12–14 (see text for details). Also shown for reference is the time series of VT_{max} for Experiment 1 and the uncapped counterpart of Experiment 14.

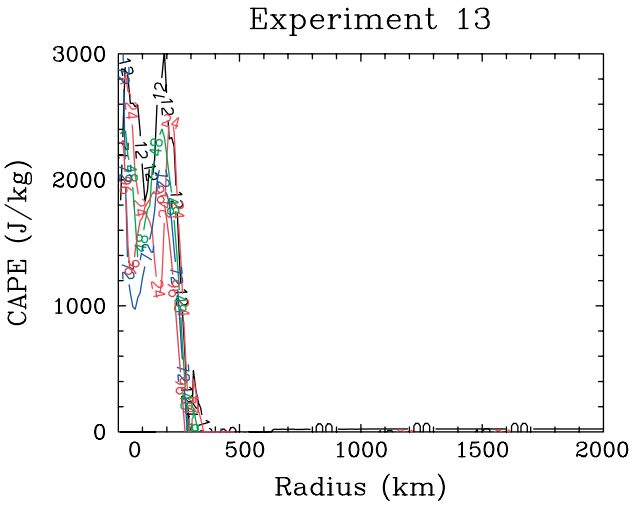

Figure A.4. Radial profiles of surface-based CAPE for Experiment 13, averaged azimuthally around the storm centre at 0, 12, 24, 48, 72 and 96 hours. This figure is available in colour online at www.interscience.wiley.com/journal/qj

in Experiment 12 is generally higher than that in Experiment 1. The vortex in Experiment 13 intensifies a little more slowly than the corresponding uncapped Experiment 12. The intensities in Experiments 12 and 13 are nonetheless comparable between 60 and 66 hours. The maximum latent heat flux for Experiment 13 is comparable to that reported in Experiment 3 (not shown).

Unlike Experiments 12 and 13, which spin up rapidly during the first eight hours after the gestation interval, Experiment 14 evidences a gradual intensification until approximately 60 hours at which time the vortex undergoes a rapid intensification to an intensity comparable to that of Experiment 13 by 96 hours. The simulated vortex clearly intensifies despite an initially neutral sounding and capped fluxes of latent and sensible heat.[§§] Also plotted in Figure A.3 is the uncapped analogue of Experiment 14. It is clearly evident that the uncapped simulation intensifies more rapidly after 48 hours, and the mature intensity is considerably stronger than its capped counterpart at 4 days. These differences between the capped and uncapped evolution are quite unlike the three-dimensional Experiments 12 and 13, indicating that in a strictly axisymmetric framework the evaporation–wind feedback mechanism adds a considerable augmentation to the spin-up on time-scales of a few days.

To address the matter of the evolution of CAPE during Experiment 13, we plot in Figure A.4 the surface-based CAPE averaged azimuthally around the storm centre. As in Figure 13, the CAPE is plotted as a function of radius at 0, 12, 24, 48, 72 and 96 hours. By design, the CAPE in the vortex environment ($r > 300$ km) remains close to zero for the duration of the simulation. At radii less than 300 km, however, the latent heat fluxes significantly moisten the surface layer with a concomitant increase of CAPE. This occurs even with the 10 m s^{-1} cap in the surface wind speed. The generation of CAPE in the core region is thus solely associated with the limited region of moisture fluxes within 300 km radius. As in section 3.2, an examination of soundings during the intensification period (not shown) confirms also a local CAPE of approximately from 400 to 600 J kg^{-1} between the moist adiabats through the VHTs and the local axisymmetric environment.

This experiment isolates clearly the VHT pathway for tropical cyclone intensification. It demonstrates that intensification is not essentially dependent on the supply of CAPE from the vortex environment. Intensification to a vortex similar in strength to that in the control experiment can occur in an initially neutral environment without the windspeed–moisture feedback process of WISHE.

The results of Experiments 12–14 lend strong support to our conclusion that the evaporation–wind feedback mechanism is not essential for tropical cyclone intensification, even when commencing with a nearly neutral sounding or suppressing any heat fluxes in the vortex environment and limiting altogether the wind speed in the heat fluxes in the vortex region. This conclusion is independent of axisymmetric or three-dimensional configurations.

[§§]This sensitivity experiment was not considered in either the Rotunno and Emanuel (1987) or the Craig and Gray (1996) studies.

References

Asnani GC. 2005. *Tropical Meteorology*. Vol. 2. Chapter 9, Tropical cyclones. Indian Institute of Tropical Meteorology: Pune, India.

Barnes GM, Zipser EJ, Jorgensen D, Marks FD. 1983. Mesoscale and convective structure of a hurricane rainband. *J. Atmos. Sci.* **40**: 2125–2137.

Betts AK, Bartlo J. 1991. The density temperature and the dry and wet virtual adiabats. *Mon. Weather Rev.* **119**: 169–175.

Black PG, D'Asaro EA, Drennan WM, French JR, Niiler PP, Sanford TB, Terrill EJ, Walsh EJ, Zhang JA. 2007. Air-sea exchange in hurricanes: Synthesis of observations from the coupled boundary layer air-sea transfer experiment. *Bull. Am. Meteorol. Soc.* **88**: 357–374.

Bolton D. 1980. The computation of equivalent potential temperature. *Mon. Weather Rev.* **108**: 1046–1053.

Braun SA. 2002. A cloud-resolving simulation of Hurricane Bob (1991): Storm structure and eyewall buoyancy. *Mon. Weather Rev.* **130**: 1573–1592.

Braun SA, Tao W-K. 2000. Sensitivity of high-resolution simulation of Hurricane Bob (1991) to planetary boundary-layer parameterizations. *Mon. Weather Rev.* **128**: 3941–3961.
Carrier GF, Hammond AL, George OD. 1971. A model of the mature hurricane. *J. Fluid Mech.* **47**: 145–170.
Craig GC, Gray SL. 1996. CISK or WISHE as a mechanism for tropical cyclone intensification. *J. Atmos. Sci.* **53**: 3528–3540.
Dudhia J. 1993. A non-hydrostatic version of the Penn State-NCAR mesoscale model: Validation tests and simulation of an Atlantic cyclone and cold front. *Mon. Weather Rev.* **121**: 1493–1513.
Emanuel KA. 1986. An air-sea interaction theory for tropical cyclones. Part I: Steady state maintenance. *J. Atmos. Sci.* **43**: 585–604.
Emanuel KA. 1989. The finite-amplitude nature of tropical cyclogenesis. *J. Atmos. Sci.* **46**: 3431–3456.
Emanuel KA. 1994. *Atmospheric convection*. Oxford University Press: Oxford, UK.
Emanuel KA. 1995. Sensitivity of tropical cyclones to surface exchange coefficients and a revised steady-state model incorporating eye dynamics. *J. Atmos. Sci.* **52**: 3969–3976.
Emanuel KA. 1997. Some aspects of inner-core dynamics and energetics. *J. Atmos. Sci.* **54**: 1014–1026.
Emanuel KA. 2003. Tropical cyclones. *Ann. Rev. Earth Planet. Sci.* **31**: 75–104.
Emanuel KA, Neelin JD, Bretherton CS. 1994. On large-scale circulations in convecting atmosphere. *Q. J. R. Meteorol. Soc.* **120**: 1111–1143.
Frisius T. 2006. Surface-flux-induced tropical cyclogenesis within an axisymmetric atmospheric balanced model. *Q. J. R. Meteorol. Soc.* **132**: 2603–2623.
Gray SL, Craig GC. 1998. A simple theoretical model for the intensification of tropical cyclones and polar lows. *Q. J. R. Meteorol. Soc.* **124**: 919–948.
Grell GA, Dudhia J, Stauffer DR. 1995. 'A description of the fifth generation Penn State/NCAR mesoscale model (MM5)'. Tech. Note TN-398+STR, NCAR: Boulder, USA.
Hack JJ, Schubert WH. 1986. Nonlinear response of atmospheric vortices to heating by organized cumulus convection. *J. Atmos. Sci.* **43**: 1559–1573.
Hendricks EA, Montgomery MT, Davis CA. 2004. On the role of 'vortical' hot towers in formation of tropical cyclone Diana (1984). *J. Atmos. Sci.* **61**: 1209–1232.
Holton JR. 2004. *An introduction to dynamic meteorology*. Academic Press: London.
Houze RA Jr. 1993. *Cloud dynamics*. Academic Press.
Hsie E-Y, Anthes RA, Keyser D. 1984. Numerical simulation of frontogenesis in a moist atmosphere. *J. Atmos. Sci.* **41**: 2581–2594.
Lighthill MJ. 1998. Fluid mechanics of tropical cyclones. *Theoret. Comput. Fluid. Dyn.* **10**: 321.
Molinari J, Vollaro D, Corbosiero KL. 2004. Tropical cyclone formation in a sheared environment: A case study. *J. Atmos. Sci.* **61**: 2493–2509.
Montgomery MT, Nicholls ME, Cram TA, Saunders AB. 2006. A vortical hot tower route to tropical cyclogenesis. *J. Atmos. Sci.* **63**: 355–386.
Nguyen SV, Smith RK, Montgomery MT. 2008. Tropical-cyclone intensification and predictability in three dimensions. *Q. J. R. Meteorol. Soc.* **134**: 563–582.
Ooyama KV. 1969. Numerical simulation of the life cycle of tropical cyclones. *J. Atmos. Sci.* **26**: 3–40.
Ooyama KV. 1997. Footnotes to 'Conceptual evolution'. Pp 13–18 in Preprints for 22nd Conf. on Hurricanes and Tropical Meteorology, Fort Collins, CO. Amer. Meteorol. Soc: Boston.
Persing J, Montgomery MT. 2003. Hurricane superintensity. *J. Atmos. Sci.* **60**: 2349–2371.
Powell MD. 1990. Boundary-layer structure and dynamics in outer hurricane rainbands. Part II: Downdraft modification and mixed layer recovery. *Mon. Weather Rev.* **118**: 918–938.
Rotunno R, Emanuel KA. 1987. An air-sea interaction theory for tropical cyclones. Part II: Evolutionary study using a nonhydrostatic axisymmetric numerical model. *J. Atmos. Sci.* **44**: 542–561.
Saunders AB, Montgomery MT. 2004. 'A closer look at vortical hot towers within a tropical cyclogenesis environment'. Paper No. 752, Atmospheric Science Bluebook. Colorado State University: Fort Collins.
Shin S, Smith RK. 2008. Tropical-cyclone intensification and predictability in a minimal three-dimensional model. *Q. J. R. Meteorol. Soc.* **134**: 1661–1671.
Smith RK. 2003. A simple model of the hurricane boundary layer. *Q. J. R. Meteorol. Soc.* **129**: 1007–1028.
Smith RK. 2006. Accurate determination of a balanced axisymmetric vortex. *Tellus* **58A**: 98–103.
Smith RK, Montgomery MT. 2008. Balanced boundary layers used in hurricane models. *Q. J. R. Meteorol. Soc.* **134**: 1385–1395.
Smith RK, Vogl S. 2008. A simple model of the hurricane boundary layer revisited. *Q. J. R. Meteorol. Soc.* **134**: 337–351.
Smith RK, Montgomery MT, Zhu H. 2005. Buoyancy in tropical cyclone and other rapidly rotating atmospheric vortices. *Dyn. Atmos. Oceans* **40**: 189–208.
Smith RK, Montgomery MT, Nguyen SV. 2009. Tropical cyclone spin-up revisited. *Q. J. R. Meteorol. Soc.* **135**: 1321–1335.

DOI: 10.1002/qj